DETERMINATION OF CRITICAL GAS SATURATION AND RELATIVE PERMEABILITIES RELEVANT TO THE DEPRESSURISATION OF THE STATFJORD FIELD

E.B. Petersen Jr[1], G.S. Agaev[1], B. Palatnik[1],
J.K. Ringen[1], P.E. Øren[1] and K.O. Vatne [2]
[1] Statoil ASA and [2] RF-Rogaland Research

This paper was prepared for presentation at the International Symposium of the Society of Core Analysts held in Abu Dhabi, UAE, 5-9 October, 2004

ABSTRACT

Depressurisation of waterflooded reservoirs can economically increase recovery and extend the life of mature fields, where mobilization of gas has been found to have a significant impact on both the oil and gas production profiles. This paper describes the determination of critical gas saturation and relative permeabilities relevant to the planned depressurisation of the Statfjord Field. A series of reservoir condition depletion experiments and associated numerical simulations are presented.

Several experiments using reservoir core and reservoir fluids were conducted to measure critical gas saturation and to determine the relative permeability functions during depressurisation. The study includes low rate depletion experiments on both virgin, limited waterflooded and extensively waterflooded samples. History matching of the experiments was used to gain information about relative permeability during depressurisation and to quality assure the data.

The implementation of these parameters in the full-field simulation models and the impact on oil and gas recovery during depressurisation of the Statfjord field are described. Full field simulation sensitivity and results from the reservoir uncertainty analysis is presented. The results from this study will be used to improve the understanding of the displacement processes and to reduce the risk associated with depressurisation of the Statfjord field.

INTRODUCTION

The Statfjord Field, located in the North Sea, is the largest producing oil field in Europe and production started in 1979. After eight years on plateau, oil production started declining in 1993. Since production start-up about 626 million Sm^3 oil (as of December 2003) has been produced, corresponding to a recovery of 63% of the STOIIP. The remaining economic oil reserves from the current drainage strategy, pressure maintenance by water and gas injection, are estimated to be about 28 million Sm^3. In addition to remaining oil, substantial gas volumes exist, either as gas dissolved in the residual and bypassed oil or as free gas from gas injection and some supplementary WAG injection. Depressurisation of the Statfjord Field is considered to be an option to increase the oil and

gas reserves from the field and to extend field life. The depletion of reservoir pressure below bubble point allows solution gas to liberate from the remaining oil in the reservoirs. The liberated gas will then segregate towards structural highs and create secondary gas caps, which can further be produced. To model these processes, the critical gas saturation for mobilization of gas and the associated relative permeability to gas are of utmost importance.

In recent years, a number of experimental and theoretical studies has been undertaken to study depressurisation phenomena [1]-[13]. Most studies have focused on evaluating the critical gas saturation at which gas becomes mobile under virgin conditions. Both experimental work [1]-[4], [11], [12] and theoretical scaling arguments [4], [7]-[10] have shown that the critical gas saturation is a power law function of the depletion rate. This functional relationship facilitates extrapolation of laboratory results to the pressure decline rate in the field. The critical gas saturation also depends on the gas-oil interfacial tension, which controls the nucleation process [1].

Generally, the critical gas saturations derived under waterflooded conditions are found to be larger than those for virgin systems [1], [8]. In addition to the parameters that affect the critical gas saturation under virgin conditions (i.e. depletion rate and gas-oil interfacial tension), the critical gas saturation for waterflooded conditions depends on the distribution of waterflood residual oil and the oil-water capillary pressure. The distribution of waterflood residual oil is controlled by the morphology of the pore space and the wettability of the system. To extrapolate laboratory results to field conditions, it is thus extremely important that the experiments are conducted with reservoir fluids and reservoir cores at representative wettability conditions. Furthermore, history matching of the experiments is important to obtain data free of laboratory scale artefacts and to be able to generate relative permeability curves.

To be able to make predictions for the Statfjord Field behavior, it was decided to perform laboratory studies on representative core material that as far as possible included the experience from the published data. This includes using representative reservoir core material, reservoir fluids, correct wettability, low depletion rates, varying degrees of waterflood and use of history matching to obtain high quality depletion parameters. Several depletion experiments corresponding to virgin conditions, a limited waterflood and an extensive waterflood were conducted. Different depressurisation rates were used on the same core samples to measure critical gas saturation and determine relative permeability functions. Rate dependent critical gas saturations were used to give trends that could be extrapolated to field conditions. The experimental data were implemented in full field reservoir simulation to test the sensitivity of the parameters.

EXPERIMENTAL

Apparatus

A simplified schematic of the pressure depletion apparatus is shown in Figure 1. The main parts of the apparatus are the pumping system, the visual sapphire cell separator and the vertically positioned core holder. The pumping system consists of three computer-controlled cylinders. During pressure depletion cylinder A was controlling the pore pressure, cylinder B adjusting the volume in cylinder A when necessary and Cylinder C the confining pressure. The depletion rate and the net confining pressure were controlled within 0.05 bar accuracy. Cylinder A and B were also used for recirculation of equilibrated fluid through the core before and after the test to measure permeability. The visual sapphire cell was placed directly on top of the vertical core holder at test conditions and was acting as a two and three phase separator as well as a visual cell to detect gas break through. The experimental system

Figure 1: Depletion

was optimized to run several samples in parallel to increase the amount of high quality data in a short timeframe. Two apparatuses of this type were run in parallel.
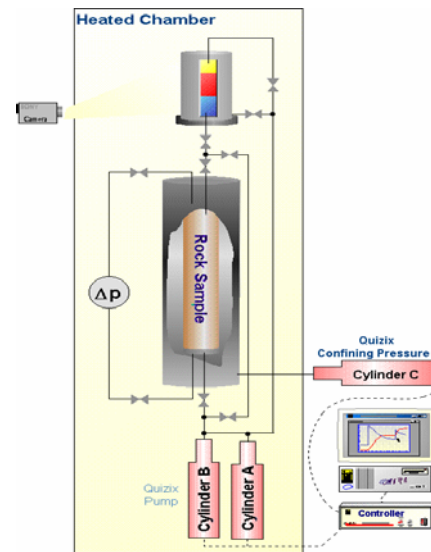
Core and fluid

Eighteen experiments have been conducted on two composite core samples from the Brent Group in the Statfjord Field. The samples were relatively homogenous, horizontal, well-consolidated sandstone plugs from two different formations. In order to obtain a representative reservoir fluid, separator oil and gas were sampled at the platform test separator. The reservoir fluid was recombined to the original bubble point pressure, 271.5 bar at 91.1 ^{0}C. Table 1 describes the core properties and conditions during depressurisation.

Table 1: Core and conditions during depletion

Core assembly	A	B
Length of core assembly (cm)	40.95	34.30
Diameter (cm)	3.75	3.76
Porosity (frac.)	0.320	0.306
Pore volume (cc)	143.0	114.4
Ko(Swi) (mD) after ageing	990	711
Swi (frac.)	0.179	0.173
Conditions Depressurisation		
Net confining pressure (bar)	150	150
Temperature (^{o}C)	91.1	91.1
Depressuration start pressure (bar)	290	290
Bubble point pressure (bar)	271.5	271.5
Depressuration end pressure (bar)	80	80

Core preparation

The individual plugs were cleaned with hot solvents and miscible saturated with formation water. The plug pore volumes were then measured by performing a miscible displacement of chloride brine with nitrate brine together with Mohr's titration. Establishment of Swi was done with porous plate drainage and Ko(Swi) measured on single plugs. To obtain an acceptably large pore volume and length, several plugs were butted together to a composite core. The plugs for each assembly were selected on the basis of matching porosity, absolute permeability and pore size distribution. The composite cores were assembled with decreasing permeability from top to bottom and Ko(Swi) was measured at different stages up to reservoir conditions. The cores were aged with reservoir oil at reservoir conditions for minimum 4 weeks. A special core analysis program was run in parallel to gain information about capillary pressure, relative permeability and wettability.

Depletion experiments

The depletion was conducted by continuously extracting fluid from the top of the vertically oriented core while keeping the net confining pressure constant. Fluids were extracted by adjusting the pressure to give a linear pressure decline with time. Each core was depleted with three different depletion rates; first at virgin conditions, then after extensive waterflooding and finally after limited waterflooding. The following three depletion rates were used: Low Rate Depletion (LRD) 0.33 bar/h, Medium Rate Depletion (MRD) 0.86 bar/h and High Rate Depletion (HRD) 2.1 bar/h. A detailed test procedure of the depressurisation program is given Table 2.

Table 2: Test procedure

Depressurisation Experiments in Chronological order.	
No. Experiment	**Description**
1 **Low rate depletion at Swi**	Fluid extracted from top of the core. Constant net confining pressure. Gas production visually detected and measured in a sapphire cell close to outlet. Low depletion rate of 8.01 bar/day from 320 to 80 bar within 629 hours.
2 **Gas permeability**	Equilibrium gas flooded from bottom of core to measure gas permeability after depletion experiment.Low flowrate (0.3 ml/min) and then high flowrate (3 ml/min). Liquid production measured in the sapphire cell.
3 **Resaturate with reservoir oil**	STO injected to displace gas and to bring the core to reservoir pressure. STO miscibly displaced with reservoir oil. Ko(Swi) measured.
4 **High rate depletion at Swi**	High rate depletion at Swi (50.4 bar/day) by repeating action number 1, 2 and 3.
5 **Medium rate depletion at Swi**	Medium rate depletion at Swi (20.7 bar/day) by repeating action number 1, 2 and 3.
6 **Relative permeability measurement**	Unsteady state technique. Water flood at 100 ml/h from the bottom with core in vertical position. Rate increased to 400 ml/h. Relative permeability curves determined with JBN technique and simulation.
7 **Low rate depletion at Sor**	Similar to action point 1
8 **Gas permeability**	Similar to action point 2
9 **Resaturate with reservoir oil**	Similar to action number 3. Measurement of oil saturation included.
10 **Establish Sor**	Water flood at 100 ml/h from bottom with core in vertical position. Rate was increased to 400 ml/h.
11 **High rate depletion at Sor**	High rate depletion at Sor (50.4 bar/day) was performed by repeating action number 7, 8, 9 and 10.
12 **Medium rate depletion at Sor**	Medium rate depletion at Sor (20.7 bar/day) was performed by repeating action number 7, 8 and 9.
13 **Limited waterflood**	Water flood at 40 ml/h from bottom with core in vertical position and stopped directly after break through.
14 **Low rate depletion after limited waterflood**	Low rate depletion (8.01 bar/day) was performed by repeating action number 7, 8, 9 and 13.
15 **High rate depletion after limited waterflood**	High rate depletion (50.4 bar/day) was performed by repeating action number 7, 8, 9 and 13
16 **Medium rate depletion after limited waterflood**	Medium rate depletion after limited waterflood (20.7 bar/day) was performed by repeating action number 7 and 8.
17 **Water content measurement**	The water content was collected in graduated test tubes during blow down and vacuum distillation. The measured volumes were corrected for salinity, temperature, pressure and hold-up volumes.
18 **Hot solvent cleaning**	Alternating flood with formation water, methanol and toluene at 7 bar and 60 ^{o}C.
19 **Pore volume, gas**	Determine pore volume with helium gas expansion and Boyles law.

At the start of depletion tests at virgin condition, the cell and pumping system were completely filled with reservoir oil. A reference test was performed with the core closed off to measure gas liberated from the separator oil during pressure depletion. This was also calculated from PVT data, and the production data during the pressure depletions of the core was corrected for gas liberated from separator oil below bubble point. The reference test matched very well with the PVT data within experimental accuracy and no sign of supersaturation effect was observed during the test. We expect the accuracy of oil and gas production to be +/- 0.1 cc.

At the start of depletion tests after extensive and limited waterflooding, the cell and the pumping system were completely filled with reservoir water. Separator outlet was always kept at bottom ensuring that only water be removed from the separator by cylinder A. Since the bubble point of formation water is below the test pressure interval, liberated gas from water was negligible.

The dead volume between the outlet of the core sample and the visual cell was kept at a minimum, typically 0.85 cc, to reduce time delay in the production. Pore-pressure, oil and gas production were recorded throughout the experiments. Water, oil and gas saturation in the core was calculated from these measurements together with PVT-values and the amount of oil in the core at start of depletion. The critical gas saturation was determined by comparing the measured production data with the PVT-trend line. Deviation of the measured gas saturation profile from the PVT-trend line indicated the point when gas left the core. As a quality control a video camera was monitoring the visual cell observing the first gas bubble leaving the core.

EXPERIMENTAL RESULTS
A summary of the key results from the depressurisation study is given in Table 3. The measured critical gas saturation ranged from 5.3 to 13.4 percent, depending on depressurisation rates and initial oil saturation. The data have been compared with published data from tests carried out on both virgin and waterflooded conditions. Figure 2 shows a plot of pressure decline rates versus measured critical gas saturation at virgin conditions. The results are in excellent agreement with the reference Brent UK data [3], [4]. A trend line has been drawn through the experimental data to a field pressure decline rate of 40bar/year giving a critical gas saturation estimate of 5 percent.

Figure 3 shows a plot of normalised pressure decline rates versus measured critical gas saturation at waterflooded conditions. The pressure decline rates have been normalised by the bubble point pressures. We observe that the critical gas saturation is slightly lower for the waterflooded case than for the virgin case. Included in Figure 3 are also relevant reference data carried out on North Sea core samples [1], [11]. Compared to the reference data the Statfjord-Brent critical gas saturation stabilised at significantly lower values than for the reference data. This can readily be explained in terms of wettability. Whilst the majority of the reference data stem from water wet samples, the samples in the present study all displayed a mixed wet behaviour with Amott Harvey indices close to zero.

In water wet samples, the residual oil exists as isolated oil ganglia. Buoyancy effects during depressurisation can be greatly reduced when gas evolves within isolated oil ganglia. Although gas may migrate relatively quickly to the top of individual oil ganglia, the large values of the oil-water and gas-water capillary pressure quickly arrest the gas migration. Consequently, the critical gas saturation increases. In a mixed wet or oil wet sample, on the other hand, the presence of oil films in the corners of water invaded pores greatly increases the continuity of the waterflooded oil. Furthermore, compared to water wet systems, the oil-water capillary pressure is reduced in mixed wet or oil wet samples. Both the increased oil continuity and the reduced oil-water capillary pressure facilitate upward migration of gas and thus lower critical gas saturation.

 The logarithmic relationship between critical gas and pressure decline rate for reference 1 and 11 is included in the figure. The same slope has been used for trend lines through sample A and B, which enables extrapolation to field pressure decline rates. For the Statfjord Brent core samples an estimate of 2 to 4 percent is obtained.

Figure 4 and figure 5 shows ternary diagrams of the trajectories for all the eighteen experiments carried out on the two Brent Group core samples; average saturation of the three phases at different times during the depressurisation.

Table 3:Main Results Depressurisation Experiments

Depressurisation	Virgin condition		At Sor		Limited WF	
Core Sample	A	B	A	B	A	B
Depressurisation rate, LRD (bar/h)	0.33	0.33	0.33	0.33	0.33	0.33
So (frac.)	0.821	0.827	0.131	0.142	0.381	0.269
Critical gas saturation (frac.)	0.083	0.107	0.053	0.095	0.064	0.067
Ultimate gas saturation	0.217	0.177	0.112	0.153	0.21	0.216
USS Gas Injection Krg (frac.)	0.058	n.m.	0.032	0.038	n.m.	0.010
Sg, end (frac.)	0.283	n.m.	0.267	0.373	0.265	0.317
Depressurisation rate, MRD (bar/h)	0.86	0.86	0.86	0.86	0.86	0.86
So (frac.)	0.821	0.827	0.148	0.145	0.422	0.412
Critical gas saturation (frac.)	0.086	0.084	0.054	0.082	0.091	0.101
Ultimate gas saturation	0.227	0.248	0.105	0.142	0.237	0.331
USS Gas Injection Krg (frac.)	0.042	0.048	0.021	0.024	0.01	0.012
Sg, end (frac.)	0.294	0.344	0.203	0.270	0.267	0.435
Depressurisation rate, HRD (bar/h)	2.1	2.1	2.1	2.1	2.1	2.1
So (frac.)	0.821	0.827	0.183	0.197	0.405	0.345
Critical gas saturation (frac.)	0.122	0.134	0.071	0.105	0.077	0.107
Ultimate gas saturation	0.256	0.268	0.141	0.199	0.234	0.252
USS Gas Injection Krg (frac.)	0.050	0.0432	0.022	0.036	n.m.	0.014
Sg, end (frac.)	0.324	0.323	0.250	0.348	n.m	0.349

COREFLOOD SIMULATION

Numerical model

Numerical simulation was used to history match the experimental output to gain information about relative permeability during the depressurisation and to quality assure the data. The experiments were modelled using a one dimensional Black-Oil simulation model (Eclipse 100). The core flood assembly consisted of six core plugs (Sample A) and five core plugs (sample B) butted together and oriented vertically with the outlet at the top. Each section was divided into 50 numerical blocks resulting in a total of 300 (sample A) and 250 (Sample B) grid blocks. To model the boundary at the top an additional block is added to the numerical model, where relative permeabilities are straight lines and capillary pressures are zero. A well was located in this block. A total reservoir volume production rate was specified for the production well.

Model input functions for relative permeabilities (normalized Corey curves) and capillary pressures (J-functions) were altered to obtain best match between simulation results and experimental data. The initial flow parameters used in the model were based on measurements on the test sample itself and neighbouring samples. In addition, flow parameters were created from network models of reconstructed pore-space samples. Input for the reconstruction, such as grain size distribution, intergranular porosity, etc., were estimated from digitized thin sections taken from the two core samples [14]. To specify capillary pressures, two J-functions, one for oil/water and one for oil/gas, were input to the model together with surface tensions. The relation is used to compute capillary pressure, which will vary with position since the experimental core is composed of several sections with different rock characteristics. End point scaling was used to restrict the mobile saturation intervals.

Matching procedure

The initial and bubble point pressures were set to 320 and 271.5 bar, respectively. Initial water saturation was set to the experimental average initial saturation in all blocks. First, the total reservoir volume production rate was adjusted to match measured outlet pressure drop. Next, sensitivity runs were performed to identify the parameters having the strongest influence on simulated results.

History match at Virgin conditions

All three depressurisation rates, LRD, MRD and HRD, for core samples A and B were history-matched. The results were most sensitive to gas relative permeability and critical gas saturation. The final match was based on running the simulation with different combination of the two most sensitive parameters.

Core sample A: The critical gas saturation was set to the experimental determined value and the relative permeability to gas was altered until the simulated data matched the experimental data. A Corey exponent of 3.3 gave excellent match for all the three depletion rates. In Figure 6 the average gas saturation in the core is compared with the simulated gas saturation. Comparison of the measured and simulated pore pressure versus time is illustrated in Figure 7.

Core sample B: The same procedure was used as for sample A. A reasonable match for all three-depressurisation rates was obtained using a Corey exponent of 3.5. In Figure 8 the average gas saturation in the core is compared with the simulated gas saturation. Comparison of the measured and simulated pore pressure versus time is shown in Figure 9.

The best-fit Corey exponents for gas together with the measured endpoint gas relative permeabilities are illustrated in Figure 11. The measured permeabilities to gas are in good agreement with the best-fit curves for both core samples.

History match at Sor
Only the depressurisation experiments at Sor for core sample A are history-matched. The simulation results were most sensitive to oil/water capillary pressure, gas relative permeability and critical gas saturation. The simulation was very sensitive to the capillary pressure. The critical gas saturation was set close to the experimentally determined value. The oil/water capillary pressure and the relative permeability to gas were altered until the simulated data matched the experimental data. In order to achieve a reasonable match a Corey of 3.5 was used, which is consistent with other published data [13]. Figure 12 shows the capillary pressure curve that gave the best fit to the experimental data together with the secondary drainage curves obtained from network modelling and measurement on a neighbour plug. In Figure 10 the average core phase saturation for the LRD experiment is compared with the simulated phase saturation. The results for the MRD and HRD confirm the simulation parameters used during the history match of the LRD.

The best-fit Corey exponents to gas together with the measured endpoint gas relative permeabilities are illustrated in Figure 11. The measured endpoint permeabilities to gas are somewhat higher but close to the best-fit curve.

FIELD-SCALE SIMULATION
Evaluation of various field development alternatives for such a non-conventional project requires availability of an appropriate reservoir simulation model. The updated Brent Group full-field simulation model was used to evaluate the depressurisation process and to study the impact of critical gas saturation, Sgcr, and gas relative permeability, krg, on gas production. Although the favourable mobility ratio results in excellent waterflood recovery, large volumes of bypassed or virgin oil will still remain in the Brent Group reservoirs because of reservoir heterogeneity. Most of the virgin oil is expected to be trapped in relatively poor quality rock, since the waterflood and WAG injection will primarily sweep high quality rock. The oil volumes remaining in both flooded and virgin zones indicate reservoir heterogeneity and compartmentalization, and require appropriate evaluation of the depressurisation behaviour in both types of saturation zones.

Critical gas saturation. The magnitude of the critical gas saturation will determine timing for establishing gas caps and the length of gas production plateau during depressurisation. Currently a base case value of Sgcr = 10% is used for the both Brent Group and Statfjord

Formation in the reservoir model for planning purposes. To estimate the impact of the critical gas saturation, sensitivity runs were performed assuming the low, most likely and high Sgcr from the new experimental study given in Table 4. The results presented in Figure 13 demonstrate that a higher Sgcr results in a delayed gas production and a decrease in total producible gas reserves.

Gas relative permeability. The flooded and virgin zone gas relative permeability curves used for performing the full-field study of depressurisation process (pessimistic, most likely and optimistic) are described in Table 4. These curves are in fact rock curves, which were obtained directly from the laboratory data without up scaling to the full-field model scale.

Table 4: Input parameters for full-field simulation studies

Sensitivities	Critical gas $S_{gcr, \%}$	Corey exponent for K_{rg}, virgin zone	Corey exponent for K_{rg}, flooded zone
Critical gas saturation sensitivities			
Optimistic	3	3.0	3.5
Most likely	5	3.0	3.5
Pessimistic	10	3.0	3.5
Gas relative permeability sensitivities			
Optimistic	5	2.5	3.5
Most likely	5	3.0	3.5
Pessimistic	5	3.5	3.5

Each individual grid cell was assigned a relative permeability curve based on oil saturation at depressurisation start-up, when both the waterflood and WAG injection in the Brent reservoirs was stopped. The saturations and pressures for a representative watered out grid block are presented in Figure 14. The block oil saturation, So, is equal to Sor at depressurisation start-up, indicating complete waterflood sweep. As the pressure declines, the oil saturation initially increases slightly due to oil swelling until the pressure reaches the bubble point at about 270 bar. Below the bubble point, the oil starts to shrink and the gas saturation increases.

The gas liberation process during depletion for the virgin oil zone is illustrated in Figure 15. After the pressure declined to the bubble point, the gas saturation increases and the oil saturation decreases. The gas saturation continues to increase due to the oil shrinkage effect. Analysis of the field krg sensitivities presented in Figure 16 indicates that gas recovery might vary considerably depending on which krg curve is applied. For the pessimistic case, peak gas production from depressurisation will occur much later than for the most likely case. The uncertainty in krg is expected to have a marginal impact on oil production during depressurisation.

It is important to note the rock curves require up scaling before they are implemented in full-filed simulation models. The results discussed in this paper are used in the pore-to-

field up-scaling project, currently being undertaken in Statoil, to establish relative permeability curves for use in full-field models. These efforts are expected to reduce uncertainties involved, and further improve the understanding of the gas liberation processes and relative permeability relationships during depressurisation process.

CONCLUSIONS

- 18 advanced pressure depletion experiments at reservoir condition have been performed, showing good internal consistency and in agreement with published data

- Extrapolation of experimental data to reservoir depletion rates of 40 bar/year gives a critical gas saturation estimate of 5% for the virgin cases and 2 - 4 % for the waterflooded cases

- Numerical simulation gave a good match to the experimental production data for both the virgin and waterflooded cases. Gas relative permeability Corey exponents of 3.3 for virgin and 3.5 for waterflooded conditions were determined

- The full field simulation with the experimental data as input showed a large dependency on both critical gas saturation and gas relative permeability. The rock curves require up-scaling before they are implemented in the full-field simulation models

ACKNOWLEDGEMENTS

REFERENCES
1. Kortekaas, T.F.M and Poelgeest F.: "Liberation of Solution Gas During Pressure Depletion of Virgin and Water-Out Oil Reservoir". SPE 19693, San Antonio, Oct. 1989.
2. Firoozabadi, A., Ottesen, B., and Mikkelsen, M.: "Measurements of supersaturation and critical gas saturation". SPE Formation Evaluation, 337-344 (1992).
3. Ligthelm D.J, Reijnen G.C.A.M, Wit K., Weisenborn A.J., and Scherpenisse W.: "Critical Gas Saturation During Depressurisation and its Importance in the Brent Field ", SPE 38475, presented at the 1997 Offshore European Conference, Aberdeen, 9-12 September.
4. Scherpenisse W., Wit K., Zweers A.E., Shoei G. and Wolfswinkel A.: "Predicting Gas Saturation Build-up During Depressurisation of a North Sea Oil Reservoir", SPE 28842.

5. Hawes, R.I., Dawe, R.A., and Evans, R.D.: "Depressurisation of waterflooded reservoirs: The critical gas saturation". SPE/DOE 27753.
6. McDougall, S.R. and Mackay, E.J.: "The impact of pressure-dependent interfacial tension and buoyancy forces upon pressure depletion in virgin hydrocarbon reservoirs". Trans. IchemE, Vol. 76, 553-561 (July 1998).
7. Du. C. and Yortsos, Y.C.: "A numerical study of the critical gas saturation in porous medium". Transport in Porous Media, Vol 35, 205-225 (1999).
8. McDougall, S.R. and Sorbie, K.S.: "Estimation of critical gas saturation during pressure depletion in virgin and waterflooded reservoirs". Petroleum Geoscience, Vol 5, 229-233 (1999).
9. Tsimpanogiannis, I.N. and Yortsos, Y.C.: "An effective continuum model for the liquid-to-gas phase change in a porous medium driven by solute diffusion: I. Constant pressure decline rates", SPE 71502, presented at the SPE Annual Technical Conference and Exhibition held in New Orleans, LA, 30th September-3rd October, 2001.
10. Tsimpanogiannis, I.N. and Yortsos, Y.C.: "The critical gas saturation in a porous medium in the presence of gravity". J. Colloid and Interface Science, Vol 270, 388-395 (2004).
11. Naylor P., Fishloch T., Mogford D. And Smith R.: "Relative Permeability Measurements for Post-Waterflood Depressurisation of the Miller Field, North Sea", SPE 63148, SPE Annual Technical Conference and Exhibition held in Dallas, Texas, 1-4 October 2001.
12. Drummond A., Fishloch T. and Rothkopf B.: "An Evaluation of Post-Waterflood Depressurisation of the South Brae Field, North Sea", SPE 71487, SPE Annual Technical Conference and Exhibition held in New Orleans, Louisiana, 30 September-3 October 2001.
13. Goodfield M. and Goodyear S.G.: "Relative Permeabilities for Post-Waterflooded Depressurisation", SPE 83958, presented at the 2003 Offshore European Conference, Aberdeen, 2-5 September 2003.
14. Øren P.E and Bakke S.: "Process based Reconstruction of Sandstone and Prediction of Transport Properties", Transport in Porous Media, Vol 46, 311-343 (2002).
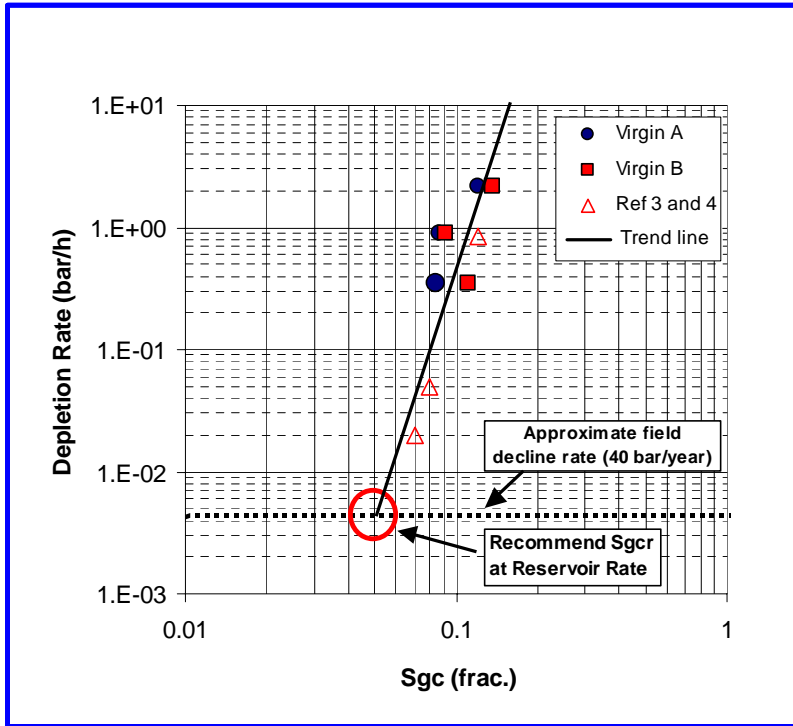
Figure 2: Comparison of critical gas saturation under Virgin conditions with Reference 3 and 4
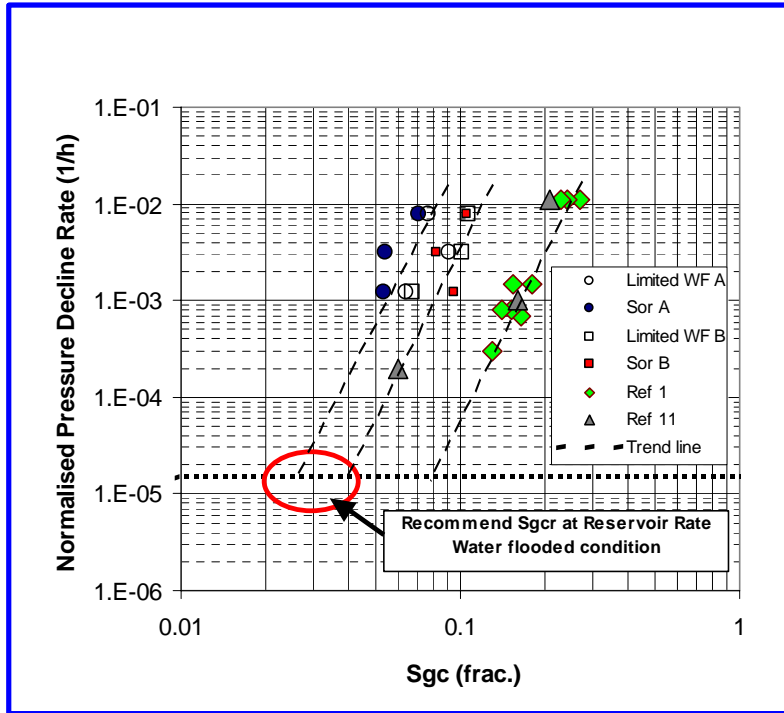
Figure 3: Comparison of critical gas saturation under Limited WF and Sor with Reference 1 and 11
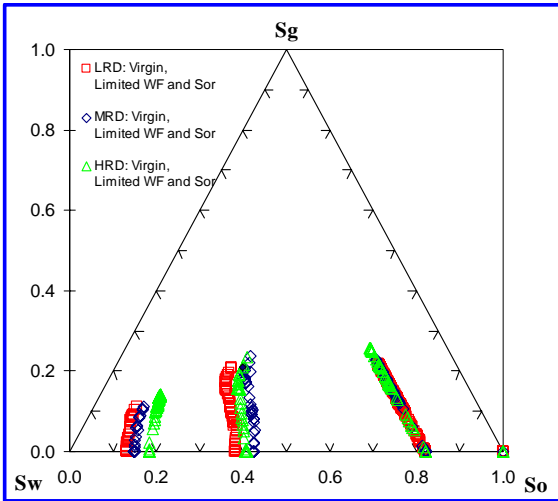

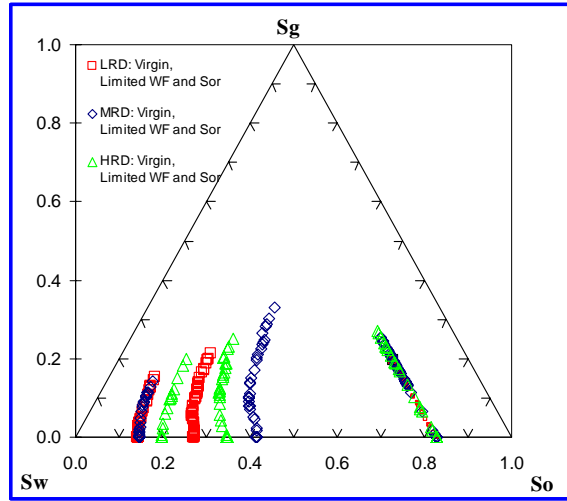Figure 4: Sample A: Saturation history during depletion at Virgin, limited WF and Sor

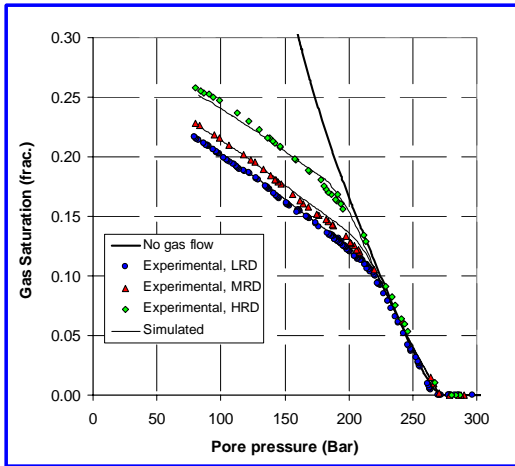Figure 5: Sample B: Saturation history during depletion at Virgin, limited WF and Sor

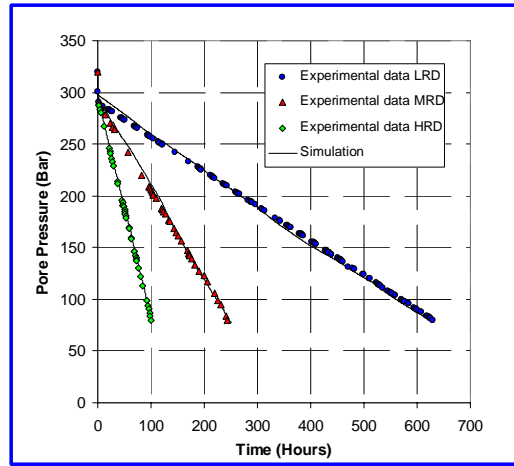Figure 6: Average Gas Saturations Sample A, Virgin Condition: Comparison of measurements and simulation

Figure 7: Average Pore Pressure vs.Time Sample A,Virgin Conditions: Comparison of measurements and simulation
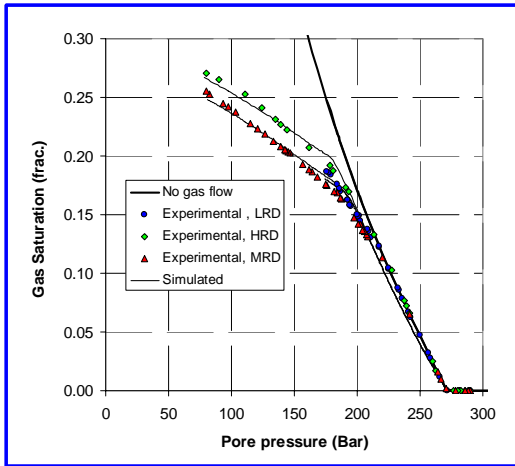
Figure 8: Average Gas Saturations Sample B, Virgin Condition: Comparison of measurements and simulation
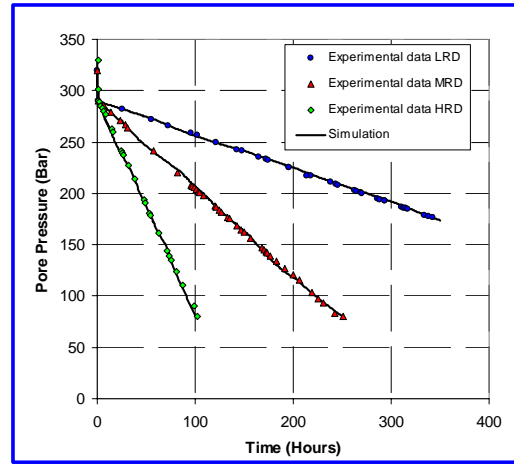
Figure 9: Average Pore Pressure vs.Time Sample B,Virgin Condition: Comparison of measurements and simulation
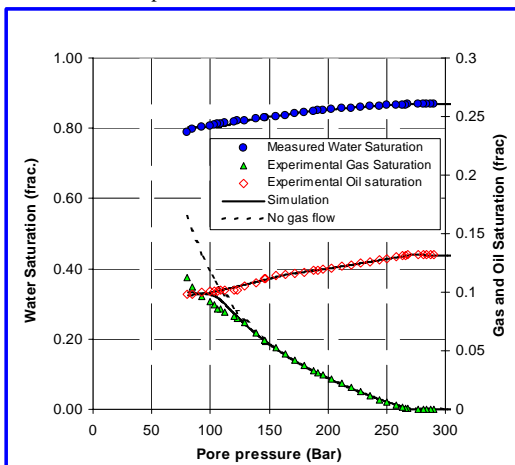
Figure 10: Average Saturation Sample A, Sor LRD: Comparison of Measurements and Simulation
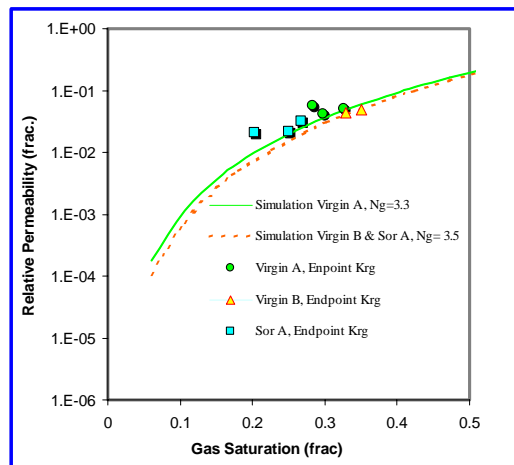
Figure 11: Gas Relative Permeability from Best-Fit simulation, Sample A and B
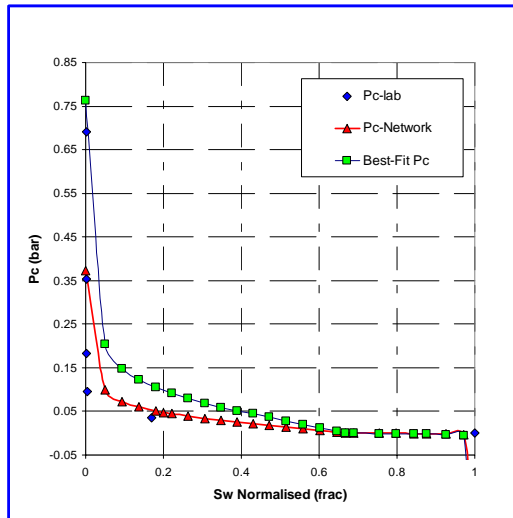
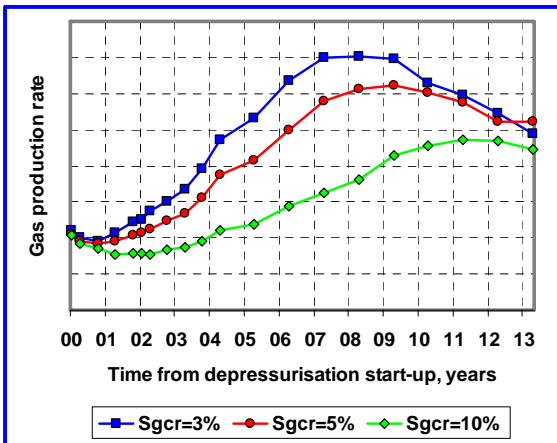Figure 12: Oil/water secondary drainage Pc curves

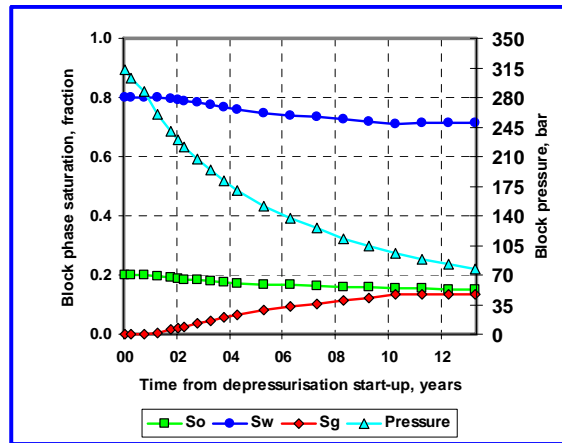Figure 13: Effect of Sgcr on Gas Production

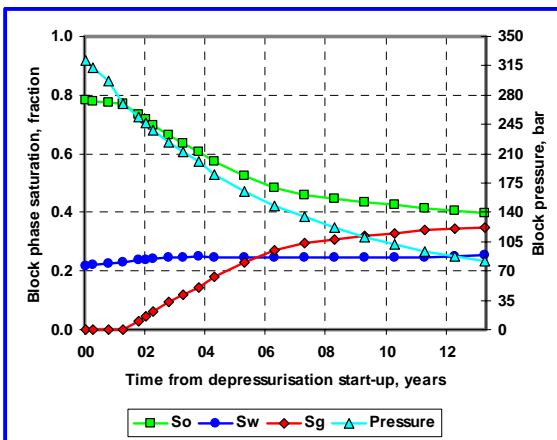Figure 14: Flooded Zone Oil Behaviour during Depressurisation
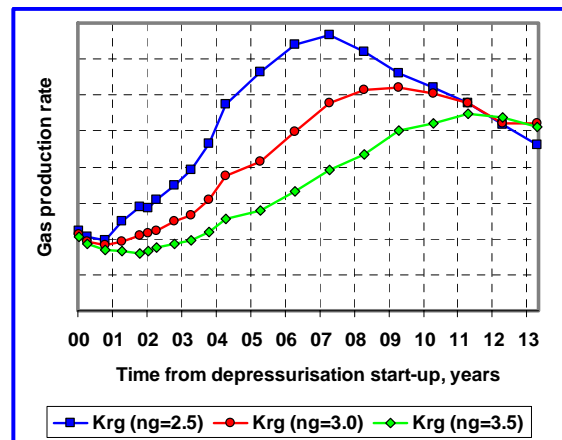

Figure 15: Virgin Zone Oil Behaviour during Depressurisation

Figure 16: Effect of Krg on Gas Production